Computer simulation of reaction-induced self-assembly of cellulose via enzymatic polymerization

2006 J. Phys.: Condens. Matter 18 S2499

(http://iopscience.iop.org/0953-8984/18/36/S20)

INSTITUTE OF PHYSICS PUBLISHING JOURNAL OF PHYSICS: CONDENSED MATTER

J. Phys.: Condens. Matter **18** (2006) S2499–S2512 doi:10.1088/0953-8984/18/36/S20

Computer simulation of reaction-induced self-assembly of cellulose via enzymatic polymerization

Toshihiro Kawakatsu[1,4], **Hirokazu Tanaka**[2,3], **Satoshi Koizumi**[2] **and Takeji Hashimoto**[2,3,4]

[1] Department of Physics, Faculty of Science, Tohoku University, Sendai 980-8578, Japan
[2] Advanced Science Research Center (ASRC), Japan Atomic Energy Agency (JAEA), Tokai, Ibaraki 319-1195, Japan
[3] Department of Polymer Chemistry, Graduate School of Engineering, Kyoto University, Katsura, Kyoto 615-8510, Japan

Received 21 February 2006
Published 24 August 2006
Online at stacks.iop.org/JPhysCM/18/S2499

Abstract

We present a comparison between results of computer simulations and neutron scattering/electron microscopy observations on reaction-induced self-assembly of cellulose molecules synthesized via *in vitro* polymerization at specific sites of enzymes in an aqueous reaction medium. The experimental results, obtained by using a combined small-angle scattering (SAS) analysis of USANS (ultra-SANS), USAXS (ultra-SAXS), SANS (small-angle neutron scattering), and SAXS (small-angle x-ray scattering) methods over an extremely wide range of wavenumber q (as wide as four orders of magnitude) and of a real-space analysis with field-emission scanning electron microscopy elucidated that: (i) the surface structure of the self-assembly in the medium is characterized by a surface fractal dimension of $D_s = 2.3$ over a wide length scale ($\sim$30 nm to $\sim$30 μm); (ii) its internal structure is characterized by crystallized cellulose fibrils spatially arranged with a mass fractal dimension of $D_m = 2.1$. These results were analysed by Monte Carlo simulation based on the diffusion-limited aggregation of rod-like molecules that model the cellulose molecules. The simulations show similar surface fractal dimensions to those observed in the experiments.

1. Introduction

In recent years we have been studying chemical-reaction-induced self-assembly of reaction products as a problem of self-assembling molecular systems in *open-nonequilibrium systems*, i.e. the systems which are subjected to energy flows. Such studies are thought to be one of the most important research topics in the 21st century, because self-assembled structures

[4] Authors to whom any correspondence should be addressed.

0953-8984/06/362499+14$30.00

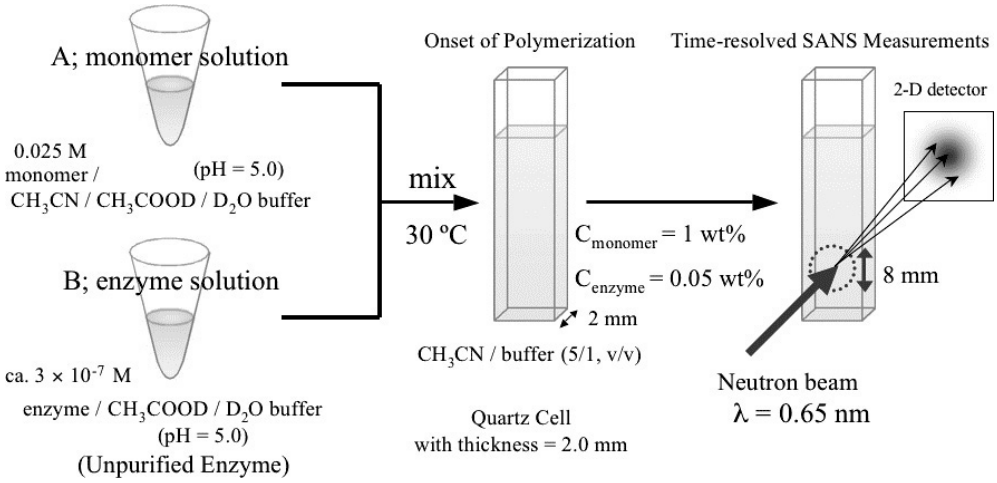

Figure 1. Experimental procedure for *in situ* small-angle neutron scattering measurements of *in vitro* synthesis of cellulose via enzymatic polymerization.

(dissipative structures), especially those on mesoscopic scales, are not well explored, despite their importance for understanding pattern formation in nature.

The system to be considered in this work consists of two stable solutions: an enzyme solution and a substrate (monomer) solution. Mixing the two solutions involves a chemical reaction in the system and hence provides energy required for an enzymatic reaction and reaction-induced self-assembly. We are interested in this reaction system not only from the viewpoint of physics on the open-nonequilibrium systems but also from the viewpoint of interdisciplinary research between chemistry (reaction at a specific site of an enzyme) and physics (self-assembly of a reaction product). When we extend the study to the *in vivo* synthesis of cellulose by bacteria [1], the research also involves biology too.

In this work, we focus on computational analyses of the experimental results obtained along this line of research. The experimental results were obtained by means of a combined Fourier-space and real-space method over a wide length scale of $\sim$30 nm to $\sim$30 μm. The computational analyses involve Monte Carlo simulation of self-assembly based on a diffusion-limited aggregation (DLA) model [2], while the Fourier-space analyses involves combined USANS (ultra-SANS), USAXS (ultra-SAXS), SANS (small-angle neutron scattering), and SAXS (small-angle x-ray scattering) methods and the real-space analyses involves field-emission scanning electron microscopy (FE-SEM).

2. Methodology

2.1. Experiments

2.1.1. In vivo enzymatic polymerization and chemical characterization. Cellulose molecules were synthesized via *in vitro* enzymatic polymerization according to the method established by Kobayashi *et al* [3]. The reaction was started by mixing two kinds of solutions A and B: A is a solution of β-cellobiosyl fluoride (monomer) and deuterated acetate buffer; B is a deuterated acetate buffer solution containing unpurified cellulase (originated from *Trichoderma viride*). After mixing A and B, the solution was syringed into acetonitrile to give a monomer concentration of 0.025 M, as shown schematically in figure 1. This was soon transferred

into a quartz cell with a thickness of 2 mm for SANS measurement, and the cell was set into a temperature enclosure controlled precisely at 30 °C. Then, immediately, time-resolved SANS measurements were carried out, as is also shown in figure 1, in order to follow the polymerization triggered by the mixing. For further details, the reader is referred elsewhere [4, 5].

At 18 h after the onset of the polymerization, where monomer conversion reaches a constant value of 75% [5, 6], the number-averaged molecular weight, M_n, of the reaction product was determined to be 1840 by size exclusion chromatography (SEC) [6], corresponding to a degree of polymerization (DP) of the repeating unit (glucose) equal to 11, and the molecular weight heterogeneity index, M_w/M_n (where M_w is the weight-averaged molecular weight) was estimated to be 1.1 [6].

2.1.2. Fourier-space analyses: a combined scattering method. In order to cover an observed length scale of self-assembly that was as wide as possible, we used a combined small-angle scattering (SAS) method of USANS, USAXS, SANS, and SAXS (from ∼30 nm to ∼30 μm). The method covers a length scale of four orders of magnitude in total. For further details, the reader is referred elsewhere [6]. In our other experiment using the WAXS technique [6], which covers the range ∼0.3 nm to ∼1.2 nm, it was revealed that the cellulose crystals formed with unpurified enzyme had the thermodynamically stable crystal structure of cellulose II [7].

2.1.3. Real-space analyses. For real-space analysis of both aggregates of enzymes (defined hereafter as 'enzyme associations') in solution B and self-assembly of the reaction product (cellulose), FE-SEM observations were performed. For this purpose, the enzyme solution and the solution of the reaction product (insoluble components with solvent) were placed on a flat silicon substrate, and solvent was evaporated gradually at room temperature under atmospheric pressure. Prior to the FE-SEM observations, the surfaces of the two samples were sputter-coated with platinum for 2 min under sufficiently low pressure. For further details, the reader is referred elsewhere [6].

2.2. Computer simulation

In order to study the real-space structure of the aggregations of cellulose on the surface of the enzyme associations on the molecular scale, we performed a series of Monte Carlo (MC) simulations of rod-like particles aggregating on a flat solid substrate. The cellulose molecule is modeled as a cylinder with length L and radius R capped with two hemispheres with radius R at both ends (the so-called spherocylinder). Although there seems to be an attractive interaction between cellulose molecules, we neglected such an interaction in the present MC simulations. An attractive interaction between cellulose molecules may lead to the formation of bundles or plates of cellulose molecules, as shown in figure 11 later. In order to incorporate such an effect into the MC simulations, the easiest way will be to adjust the aspect ratio ($2R : L + 2R$) according to the average number of cellulose molecules that form a single bundle.

The MC simulations were performed in a cubic box with sides of length $L_x = L_y = L_z$, where the x-and y-axes are set parallel to the substrate and the z-axis is perpendicular to the substrate surface. We take this side length of the simulation box to be much larger than the thickness of the aggregation layer of the cellulose molecules. We assume that the solid substrate corresponds to the plane $z = 0$ and the other boundary in the z-direction (i.e. $z = L_z$) is regarded as being essentially infinitely far from the substrate. At a randomly chosen point on the plane $z = h$ (where h is sufficiently large), we place a molecule (a spherocylinder) with its principal axis randomly oriented and let it diffuse using the standard MC procedure, as

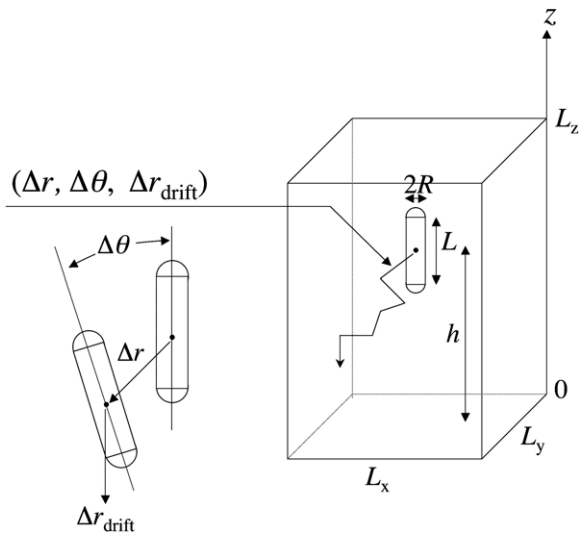

Figure 2. Schematic illustration of the system used for Monte Carlo simulation.

shown in figure 2. A single MC step consists of the following two trial motions: a translation of the centre of mass with a distance Δr in a randomly chosen direction over the whole steric angle 4π, followed by a random orientation of the axis of the cylinder (the director) with an angle $\Delta\theta$. The probability distributions of the translational distance Δr and the angular change $\Delta\theta$ are assumed to be Gaussian distributions with mean 0 and standard deviations σ_r and σ_θ, respectively. We also impose a drift motion towards the substrate surface. This drift motion reflects a concentration gradient of the synthesized cellulose molecules built up along the z-axis (the concentration being highest at $z = 0$), as will be discussed in section 3.2. Such a drift motion can be achieved by translating the centre of mass by a fixed distance $\Delta r_{\mathrm{drift}}$ at every MC step toward the negative z direction. When the molecule touches the substrate surface, its position and director is fixed. Then, we let another molecule diffuse from $z = h$ until it touches either the substrate surface or another molecule that has already been fixed. This procedure is repeated until the desired number density of molecules per surface area is achieved. Using the molecular configurations thus obtained, we calculate the scattering function $S(\mathbf{q})$ using the following formula:

$$S(\mathbf{q}) = \frac{1}{N}\left\langle \left(\sum_{i=1}^{N} \cos \mathbf{q}\cdot\mathbf{r}_i\right)^2 + \left(\sum_{i=1}^{N} \sin \mathbf{q}\cdot\mathbf{r}_i\right)^2 \right\rangle \tag{1}$$

where N is the total number of molecules in the system, $\mathbf{q}$ is the wavevector, and $\mathbf{r}_i$ is the position vector of the centre of mass of the ith molecule. We evaluate the fractal dimension using this scattering function. In comparison with experimental results, $\mathbf{q}$ and $\mathbf{r}_i$ should be considered to be reduced quantities with respect to the molecular size L, i.e. $\mathbf{q}L$ and $\mathbf{r}_i/L$.

3. Summary of experimental results and reaction-induced self-assembly

3.1. Results

Here we shall first summarize the experimental results that are either previously reported or to be published elsewhere [4–6]. The two solutions A and B before mixing were explored

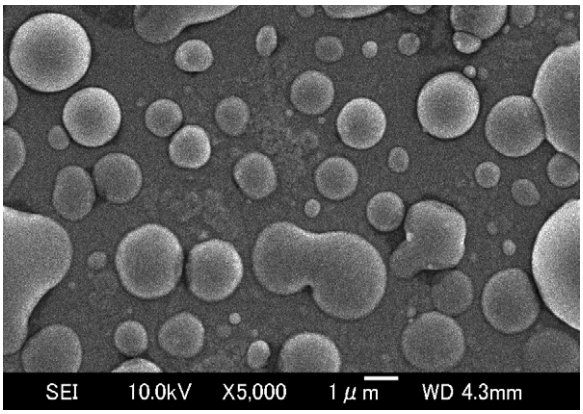

Figure 3. FE-SEM image for the enzyme associations.

by SANS to study their internal structures. The monomer solution A showed only weak scattering, which is detectable at $q > 0.06$ nm^{-1} and which is independent of q. The q-independent background scattering is due to incoherent scattering and thermal concentration fluctuations between non-deuterated acetonitrile and deuterated acetate buffer. The absence of excess scattering in the smaller q-region suggests that the monomer solution is homogeneous. However, solution B shows small-angle scattering (in a range $q < 0.1$ nm^{-1}) in excess to the q-independent background scattering at $q > 0.1$ nm^{-1} [5]. The background scattering has the same physical origin and the same intensity as that for solution A. After a correction for the background scattering, the excess scattering of solution B in terms of the differential scattering cross section $\mathrm{d}\Sigma/\mathrm{d}\Omega\,(q)$ exhibited a power law of

$$\mathrm{d}\Sigma/\mathrm{d}\Omega\,(q) \sim q^{-\alpha} \tag{2}$$

where the exponent $\alpha = 4$ [5]. The power-law scattering given by equation (2) can be rationalized by Porod's law [8], which is applicable to structures having a smooth interface with an infinitesimally thin interfacial boundary. Porod's law was observed down to the lowest accessible q of $q = 0.03$ nm^{-1}, suggesting that the enzyme associations of at least larger than 200 nm were formed in the enzyme solution. Since the enzyme (cellulase) consists of hydrophilic and hydrophobic components, their interactions with the aqueous medium may naturally give rise to the enzyme associations. The pieces of evidence reduced by the SANS profiles were confirmed by FE-SEM, as demonstrated in figure 3. The image in figure 3 elucidates the fact that enzyme associations have a smooth interface with a sharp interface boundary and a dimension greater than 200 nm.

Figure 4 shows the combined SAS scattering profiles for the reaction-induced self-assembly of the synthesized cellulose molecules measured at 18 h after the onset of polymerization where the reaction is almost completed, as evidenced by monomer conversion reaching a steady value and the surface fractal dimension D_s reaching a steady value of 2.3 [5]. The two bold lines correspond to USANS and SANS profiles, and the profiles shown by symbols correspond to USAXS and SAXS profiles. The USANS and USAXS profiles, as well as the USAXS and SANS profiles, were smoothly connected with the overlap q-ranges which are sufficiently wide. The connected scattering profiles reveal the power law (equation (2)) with its exponent $\alpha = 3.7$. Furthermore, the SANS profile is found to be connected with the SAXS profile, which exhibits a broad scattering maximum or shoulder at $q = q_m \cong 9 \times 10^{-1}$ nm^{-1}, as shown by the arrows in the figure.

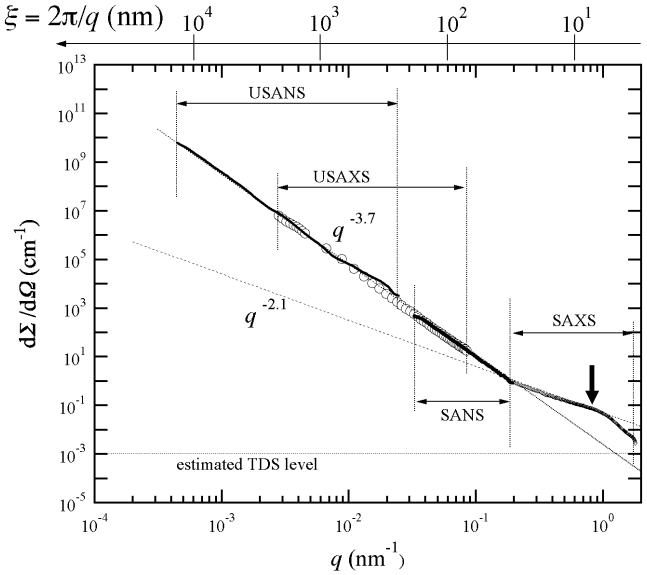

Figure 4. Combined SAS profiles for the self-assembly of synthetic cellulose. The SAXS profile was corrected for thermal diffuse scattering.

The lower cut-off wavenumber $q_{l,c}$ for the power law with $\alpha = 3.7$ is less than 4×10^{-4} nm^{-1}, and the upper cut-off wavenumber $q_{l,u}$ is $\sim 2 \times 10^{-1}$ nm^{-1}. Thus, the q-range over which the power law is applicable is as wide as about three orders of magnitude. We may be able to interpret the power-law scattering as a consequence of the self-assembly having a surface structure with respect to the aqueous medium as characterized by the surface fractal dimension of D_s [9],

$$D_s = 2d - \alpha, \tag{3}$$

where d is the space dimensionality. Since $d = 3$ and $\alpha = 3.7$, $D_s = 2.3$. The SAXS profile may also be qualitatively characterized by another power law with $\alpha = 2.1$, as shown by the dotted line in the figure, though the narrow q-range over which the power law is seen makes this assertion less certain compared with that for the power law with $\alpha = 3.7$. We may interpret the power law with $\alpha = 2.1$ as a consequence of mass fractal structure which exists inside the self-assembly. Then the mass fractal dimension $D_m = \alpha = 2.1$ [10]. The results $D_s = 2.3$ and $D_m = 2.1$ appear to suggest that the self-assembly is formed via DLA. The broad maximum or shoulder may reflect the characteristic spacing of the local structures in the assembly [11], as will be briefly discussed later in section 4.

Figure 5 shows the FE-SEM images of the self-assembly formed by the reaction products at 18 h after the enzyme reaction. The image obtained at the lowest magnification (part (a)) exhibits a rough surface having a characteristic length of $\sim$30 μm, as marked by the square in the figure, below which the surface appears to be smooth with this magnification. Part (b) shows a portion of the image marked by the square in part (a), enlarged 10 times. The image in part (b) shows a surface roughness statistically similar to that in the image in part (a). Similarly, part (c) shows a portion of the image enclosed by the square in part (b), enlarged $\sim$20 times. The image again shows a roughness similar to that of the image in part (b). The image reveals a lower cut-off length of $\sim$30 nm for the self-similar surface roughness. These results are consistent with those obtained from the combined SAS experiments.

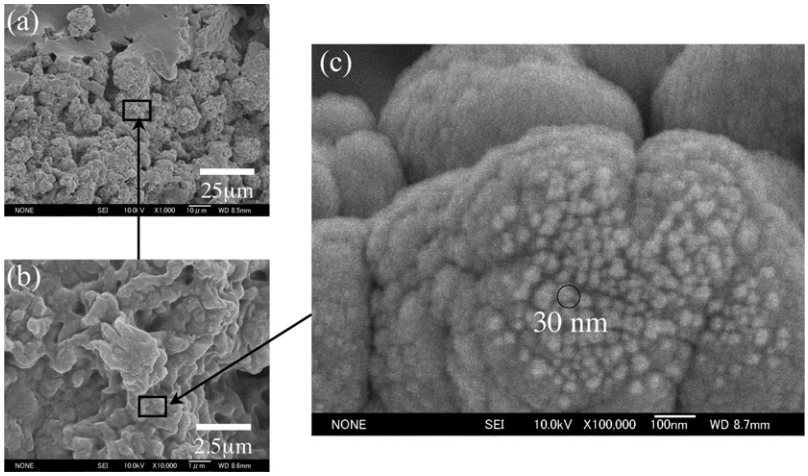

Figure 5. FE-SEM images for the self-assembly of synthetic cellulose with different magnifications.

3.2. Reaction-induced self-assembly

Based on the experimental results obtained from both Fourier-space and real-space analyses, we can now visualize the reaction-induced self-assembly of cellulose molecules at specific sites of enzymes. Figure 6 schematically presents the self-assembling process. In this work we employed an unpurified enzyme which contains only a small amount of active enzymes ($<1\%$ of the total) and a large amount of enzymes that are inactive for polymerization. The enzymes aggregate in the aqueous reaction medium, because hydrophobic interactions of enzymes outweigh their hydrophilic interactions with the aqueous medium. The enzyme associations have a flat interface over the length scale <200 nm and a sharp interface boundary, as depicted in part (a), and as evidenced by figure 3 and the SANS profile for the enzyme solution [5].

An active enzyme contains an active site consisting of one set of active subsites in a special part of the enzyme ($\sim$5 nm in diameter) of the so-called cleft, having $\sim$3 nm in length and $\sim$0.5 nm in the cross-sectional directions, where a substrate monomer is recognized and activated for polymerization (via a condensation reaction) by an active subsite, and a growing polymer chain is also recognized and anchored by another active subsite [3, 12]. The active sites in the enzyme association are expected to be statistically far apart, as shown in part (a), because unpurified enzymes were used. Driven by osmotic pressure, a monomer ($\sim$1 nm) diffuses into the active site and is recognized, activated and reacted (chemically linked via a condensation reaction) with a growing polymer chain anchored in another active subsite. After completion of this reaction cycle, another monomer that has diffused into the same active subsite enters the same reaction cycle, which may be designated a 'turnover for monomer reaction'. A polymer chain grows due to successive turnovers for monomer reaction, and then the growing polymer chain end may be brought away from the active subsite, driven by osmotic pressure, due to an increased local polymer concentration in the cleft and its surrounding space as a consequence of increased DP. The polymer chain brought away from the active subsite is terminated for polymerization, and another chain starts to grow at the same subsite, which may be designated 'turnover for polymer growth'.

A great number of polymers having a number average DP $= 11$ are created one by one from each active site in the enzyme association, as depicted in part (b), due to the two kinds of successive turnovers in the enzymatic polymerization process. As a consequence, particular

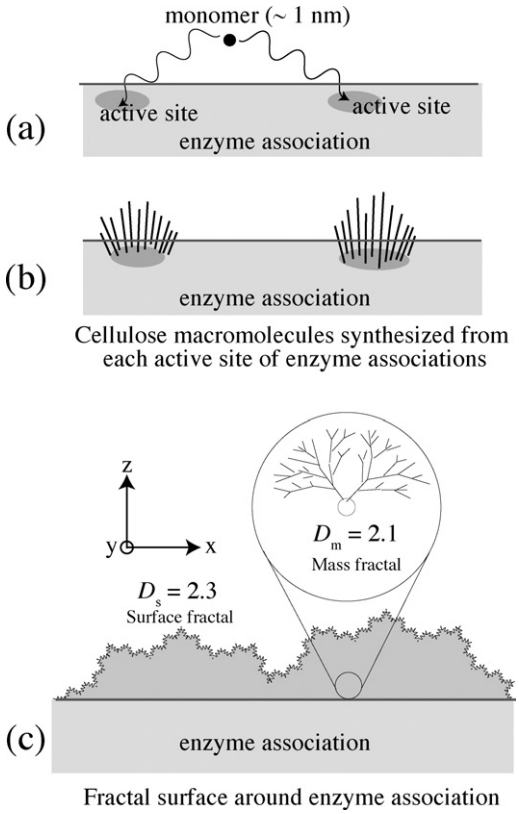

Figure 6. Schematic illustration of the self-assembly process of cellulose molecules synthesized via enzymatic polymerization.

portions of the surface of the enzyme association are enriched by polymers, which should diffuse away from the surface, driven by osmotic pressure. It should also be noted that the polymers created at active sites may be wet and spread over the surface of the enzyme association through hydrophobic interactions of cellulose molecules with hydrophobic parts of the enzymes. As a consequence, a concentration gradient of cellulose molecules will develop along the z direction, normal to the interface of the enzyme association, such that the concentration decays with z, from the interface located at $z = 0$.

The synthesized cellulose having low DP is more or less rigid and has an extended or rod-like conformation with a length of $\sim$5.5 nm and a diameter of $\sim$0.3 nm, and thus an aspect ratio of $\sim$18. The polymers cannot be dissolved in the aqueous reaction medium, and hence associate themselves into the aggregates, when they encounter each other in the reaction medium through diffusion driven by osmotic pressure, and eventually crystallize into fibrils. This reaction-induced self-assembling process driven by DLA results in the self-assembled structure having a fractal surface ($D_s = 2.3$) and mass fractal arrangement of fibrils ($D_m = 2.1$) inside the self-assembling structure, as depicted schematically in part (c). The self-assembled structures are expected to still have enough free space for the monomers to diffuse from the reaction medium into the active sites and for the dead polymers to diffuse out from the active sites through the surface of the enzyme association to the reaction medium, both driven by osmotic pressure, because the average volume fraction of polymers in the assembly is still as low as $\sim 1.5 \times 10^{-2}$,

Table 1. Parameters used in the MC simulations.

	N	L_x	L_y	Surface density	Thickness of the assembly, T [a]	Density, ρ_n [b] (molecules/ℓ)	ϕ [c] $\times 10^2$
Case I	500 000	100.0	100.0	50.0	10.3	2.9×10^{22}	1.4
Case II	200 000	100.0	100.0	20.0	3.8	3.2×10^{22}	1.5
Case III	100 000	100.0	100.0	10.0	1.8	3.3×10^{22}	1.6

[a] Average thickness of the assembly.
[b] Average density of the assembly.
[c] Volume fraction of spherocylinders in the assembly.

as will be detailed in section 4, and furthermore polymers self-assembled into the mass fractal structure, giving rise to a large space for diffusion of polymers compared to the case of uniform distribution of cellulose in the assembly.

4. Simulation results and discussion: comparison with experimental results

The MC simulations described in section 2.2 were performed for spherocylindrical molecules, with the length of the cylindrical part $L = 1.0$ nm and diameter $2R = 0.0588$ nm, both of which are reduced with respect to L (aspect ratio $(L + 2R)/(2R) = 18.0$). This aspect ratio of 18.0 of the spherocylinder is chosen on the basis of the experimental data of the cellulose molecule described in the preceding section. We performed simulations for several values of the number density of molecules per unit substrate area, as described in table 1. The parameters for the MC trial moves are $\Delta r = 0.005$, $\Delta\theta = 0.01$ rad, and $\Delta r_{\rm drift} = 0.005$, respectively. The values of the trial moves Δr, $\Delta\theta$ and $\Delta r_{\rm drift}$ are chosen to be sufficiently small so that the choice of these parameters does not affect the final results.

In figures 7(a)–(c), we show typical snapshot pictures of the aggregates for the three cases listed in table 1. These figures show parts of the total system with sizes of about 50×50 in terms of reduced units of L_x/L and L_y/L. The corresponding density profiles in the z-direction are shown in figure 8 where z is reduced with respect to L. Peaks at around $z = 0$ show local ordering of the spherocylinders due to the restrictions on their positions and directions imposed by the substrate. Using these density profiles, we define the thickness T (reduced with respect to L) of the assembly layer by the position where the density takes half the value of the plateau value in the vicinity of the substrate. The results are shown in table 1, along with other quantities such as the average number density (ρ_n) and volume fraction (ϕ) of spherocylinders in the molecular assembly.

In case I (figures 7(a) and 8) with the highest surface density of 50.0, we observe that the aggregates of molecules form a thick layer of $\sim$10.3 thickness on the substrate.

Based on the assumption that the synthesized cellulose molecules having DP = 11 (with respect to a glucose unit) are rodlike with $L = 5.5$ nm and $2R = 5.5 \times 0.0588 = 0.32$ nm, the corresponding value of ρ_n is estimated to be 500×10^3 cellulose molecules/$(100 \times 100 \times 10.3 \times 5.5^3 \times 10^{-24})\ell \cong 2.9 \times 10^{22}$ cellulose molecules/ℓ for case I. Using this value of ρ_n, the volume fraction of the cellulose molecules ϕ for case I is estimated to be $2.9 \times 10^{22} \times [\pi \times 0.0294^2 \times 1 + 4 \times \pi \times 0.0294^3/3] \times 5.5^3 \times 10^{-24} \cong 1.4 \times 10^{-2}$. The values ρ_n and ϕ for case II and case III can be similarly estimated, as given in table 1. In all the cases, the volume fraction of the cellulose molecules in the assembly is low, so that the assembly contains enough free space inside it. This situation would enable the diffusion of monomers from the reaction medium to the active sites and the diffusion of synthesized polymers from the active sites to the reaction medium.

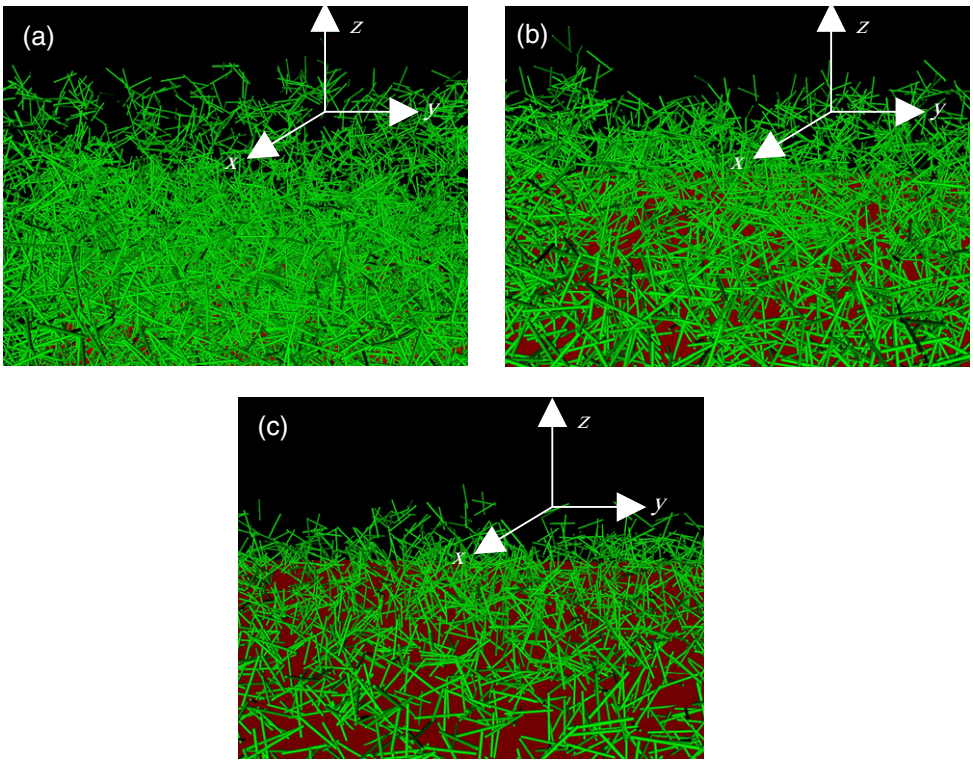

Figure 7. Snapshot pictures of the aggregates for the three cases listed in table 1; (a) case I, (b) case II, and (c) case III, respectively.

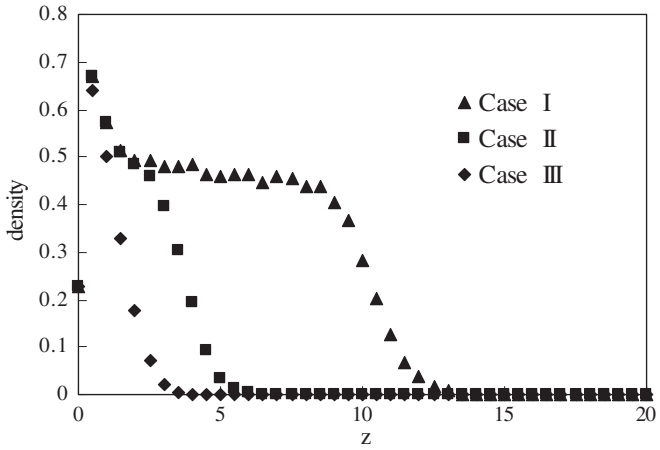

Figure 8. Density profiles in the z-direction are shown for the three cases in table 1.

We can estimate the average number density of synthesized cellulose in our experimental system, $\rho_{n,\mathrm{exp}}$, as follows: $\rho_{n,\mathrm{exp}} = 0.025 \times 0.75 \times 6.0 \times 10^{23}/5.5$ cellulose molecules/$\ell \cong 2.0 \times 10^{21}$ cellulose molecules/ℓ, from monomer concentration (0.025 M), monomer conversion (0.75) and DP of monomer (β-cellobiosyl fluoride, 5.5). This $\rho_{n,\mathrm{exp}}$ is smaller than

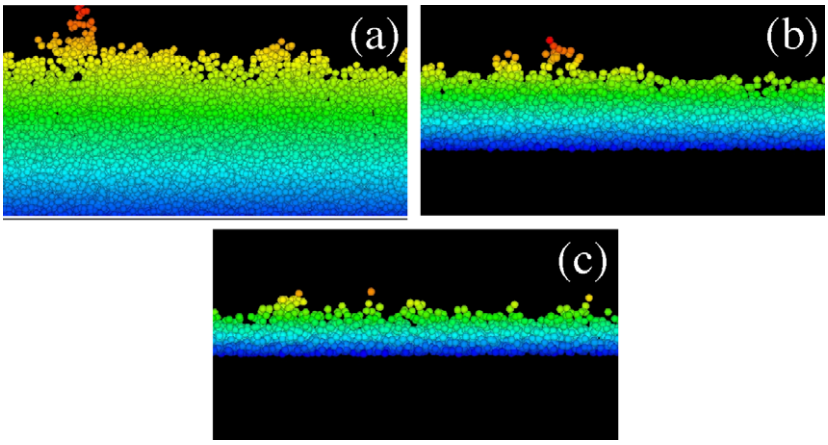

Figure 9. Cross sections of the three-dimensional structures shown in figure 7. The centres of mass of the spherocylinders are shown by small spheres with a diameter of 1.0. The region shown is a thin layer parallel to the yz plane with an area of 50.0×50.0 and a thickness of 1.0 along the x axis. Colour gradation indicates the distance from the substrate plane.

the simulation result $\rho_{\rm n} \cong 2.9 \times 10^{22}$ by a factor of $\sim$10. However, this value of $\rho_{n,\rm exp}$ is based on the assumption that cellulose molecules are dissolved uniformly in the solution. Thus the local number density of cellulose molecules in the assembly is expected to be much larger than the value $\rho_{n,\rm exp}$. Hence the value $\rho_{\rm n}$ used in the MC simulations might be close to or at least not be very different from the experimental value.

In figure 9, we show the cross sections of the aggregation layers parallel to the yz plane for the three cases in figure 7. We picked up only the particles whose centres of mass lie in the thin slab parallel to the yz plane with a thickness of $(L_x/2) - 0.5 < x < (L_x/2) + 0.5$ (in units of the molecular length L), and showed their centres of mass by small spheres with a diameter of 1.0. As the actual diameter of the spherocylinder is 0.0588, the aggregate is much more sparse than it appears in this figure. We can observe that the surfaces of the layers show fractal-like irregular structures, while the inside regions of the layers are more or less uniform.

In order to investigate the fractal dimensions of these structures, we calculated the scattering functions defined by equation (1). As this definition of the scattering function does not include the effect of the form factor originating from the spherocylindrical molecular shape, it should instead be called the structure factor. As we confirmed that neighbouring spherocylinders have negligibly small orientation correlations, the total scattering function is a product of the structure factor defined by equation (1) and the form factor of a spherocylinder times the number of spherocylinders N. The effect of the form factor appears only in the high-q region, while we discuss the large-scale fractal-like structure that is shown in the low-q region. Actually, the length of the spherocylinder that we used in the simulations is 1.0 in our dimensionless unit, which means that the form factor will affect the data only in the high-q region of $6.28 < q$. Therefore, as long as we are interested in the large-scale structures, neglecting the form factor does not cause any problems in the following discussions, and the quantity $S(q)$ defined in equation (1) can be directly compared with the scattering cross section $\mathrm{d}\Sigma/\mathrm{d}\Omega(q)$ obtained in the scattering experiments.

The calculated scattering functions are shown in figures 10(a)–(c) for the three cases in table 1. In the densest case (case I) shown in figure 10(a), the slope of the scattering function in the region $0.06 < q < 0.3$ gives -1.96, as shown by the straight line as a visual guide.

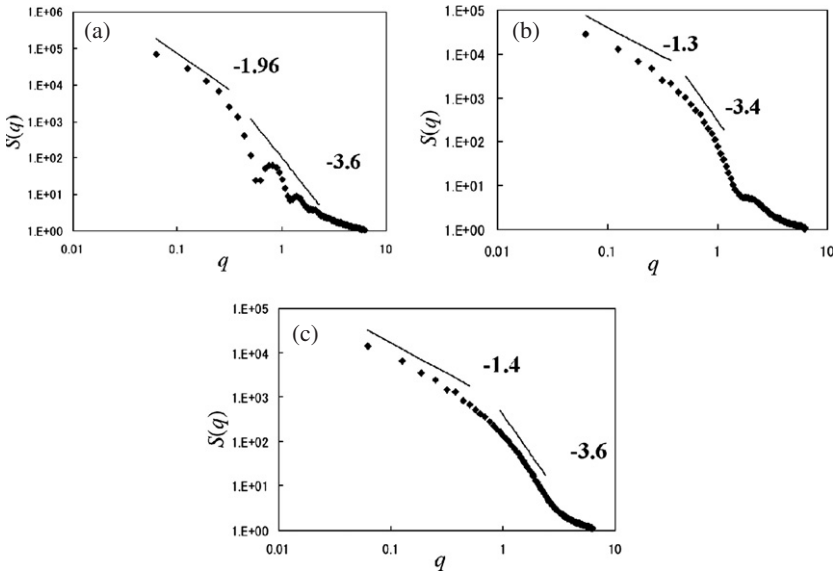

Figure 10. Scattering functions for the three cases listed in table 1.

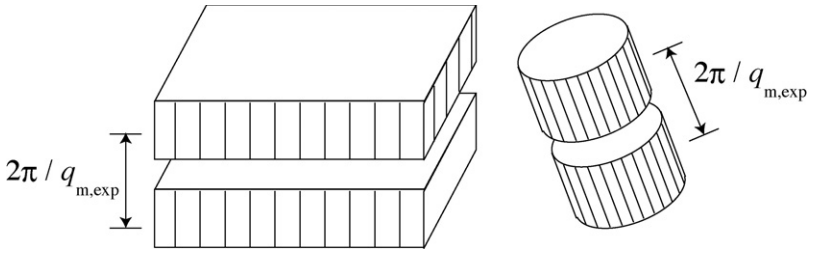

Figure 11. Local structures of cellulose aggregates.

On the other hand, we observe a series of peaks in the high-q region. These behaviours can be understood if we identify the aggregation layer as a dense uniform packing of the particles. Actually, a dense uniform layer with thickness T which is randomly oriented in three-dimensional (3D) space gives scattering in the z-direction (perpendicular to the substrate surface) as $q^{-2}\frac{\sin^2(qT/2)}{(qT/2)^2}$, which leads to the low-q behaviour as $q^{-2}\frac{\sin^2(qT/2)}{(qT/2)^2}\sim q^{-2}\mathrm{e}^{-\frac{1}{3}q^2T^2}\sim q^{-2}$ in the limit of $q \to 0$ and to a series of peaks at $qT/2 = 4.28, 7.6, 10.82, \ldots$ in the high-q region with an envelope q^{-4}. The exponent -2 in the limit $q \to 0$ is close to that -1.96. The fact that the peak positions in figure 10(a) are $q \cong 0.75$ and 1.38 implies that $T \cong 11.4$ or 11.0, which is close to the observed value $T \cong 10.3$. The slope of the envelope of these peaks is not actually -4 but closer to -3.6. This larger slope suggests a surface fractal dimension, as will be discussed in the following paragraph. An upward deviation of $S(q)$ from the power-law behaviour of $q^{-\alpha}$ ($\alpha \cong 3.6$) which is observed in the high-q region may arise from a spatial distribution of centres of spherocylinders inside the assembly. Numerical identification of these fractal dimensions using a much larger simulation system is one of the targets of our future work.

Contrary to the case I, we observe at least two different fractal dimensions for the cases II and III, as shown by the guide lines in figures 10(b) and (c). The smaller slopes in the low-q

region (-1.3 in case II and -1.4 in case III) correspond to the slope of-2 in the low-q region of case I, and should be attributed to the finite thickness of the aggregation layers. On the other hand, we observe another larger slope in the high-q region, which should be attributed to the surface fractal, as in the experimental situation discussed in the previous section. For example, we observe a slope of -3.4 ($D_s = 2.6$) within the region $0.5 < q < 1.2$ (in figure 10(b)) and a slope -3.6 ($D_s = 2.4$) within the region $0.9 < q < 2.4$ (in figure 10(c)) as shown by guide lines, which are close to the experimental value of -3.7 ($D_s = 2.3$) observed in figure 4. The low-q limit of this surface fractal region is determined by the finite thickness effect of the aggregation layers. This can be confirmed by the fact that the ratio between the lower bounds of the fractal regions in cases II and III is about 2, which is inversely proportional to the ratio of the values of the layer thickness between these two cases. On the other hand, the high-q limit of the surface fractal region may be determined by the molecular scattering.

The scattering from the surface fractal becomes very small with increasing q, as it drops according to $q^{-3.6}$ and hence it is outweighed by the scattering from a spatial distribution of the spherocylinders inside the assembly which may reflect a mass fractal structure, as inferred from the experimental result shown in figure 4. This point should be reserved for future work.

Thus, we conclude that, as the surface density of the cellulose molecules becomes smaller (as the fraction of the surface region in the aggregation layer becomes larger), the surface fractal with a fractal dimension $D_s \cong 2.4$ becomes pronounced. As has already been discussed, the slope of the envelope of the peaks in the high-q region of figure 10(a) is about -3.4, which can be attributed to the surface fractal.

5. Concluding remarks

By using the DLA model of spherocylinders, we performed a series of MC simulations of the self-assembling process of cellulose molecules polymerized on the surface of enzyme aggregation. When the surface density of the cellulose molecules on the surface of the enzyme aggregation is low, a surface fractal dimension $D_s \cong 2.4$ was observed, as in the case of the experiments. When the surface density of the cellulose molecules becomes large, such a surface fractal nature is smothered by the finite-size effect of the cellulose layers, which leads to a series of peaks. However, even in this case, the envelope of the peaks shows the same surface fractal nature.

Here we give a brief quantitative comparison between the experiments and simulations. The upper cut-off wavenumber q_u of the surface fractal region is $q_{u,\mathrm{exp}} \cong 0.2\ \mathrm{nm}^{-1}$ for the experimental case, while it is $q_{u,\mathrm{CS}} \cong 0.2\ \mathrm{nm}^{-1}$ in case II and $q_{u,\mathrm{CS}} \cong 0.4\ \mathrm{nm}^{-1}$ in case III in the simulations ($q_u L \cong 1.2$ in case II and $q_u L \cong 2.4$ in case III, with the unit of length $L = 5.5$ nm). Thus, the experiments and the simulations are consistent. On the other hand, the lower cut-off wavenumber q_l of the surface fractal region is $q_{l,\mathrm{exp}} \cong 4 \times 10^{-4}\ \mathrm{nm}^{-1}$ in the experiment, while it is $q_{l,\mathrm{CS}} \cong 0.5/5.5 = 0.09\ \mathrm{nm}^{-1}$ in case II and $q_{l,\mathrm{CS}} \cong 0.9/5.5 = 0.16\ \mathrm{nm}^{-1}$ in case III of the simulations. We can attribute this discrepancy to the finite system size effect. The position of the main peak in the high-q region q_m is $q_{\mathrm{m,exp}} \cong 0.8\ \mathrm{nm}^{-1}$ in the experiment. This peak seems to reflect the spacing between cellulose molecules. In the simulations, however, the positions of the main peaks are $q_{\mathrm{m,CS}} \cong 0.75/5.5 = 0.14\ \mathrm{nm}^{-1}$ in case I and $q_{\mathrm{m,CS}} \cong 2.14/5.5 = 0.39\ \mathrm{nm}^{-1}$ in case II. The surface density dependence of the position of the main peak implies that this main peak does not arise from the spacing between spherocylinders, because the average densities of the spherocylinders within the aggregation layers are almost the same (see table 1). Instead, we attributed these peaks to the finite sizes of the aggregation layers. So, the origin of the main peaks is different between the experiment and the simulation.

An important factor that has not yet been taken into account in the present simulation is the effect of the attractive interaction between the cellulose molecules. Such an attractive interaction leads to the formation of bundles of cellulose molecules. We may be able to consider that the $q_{\mathrm{m,exp}}$ reflects the interbundle spacing $D = 2\pi/q_{\mathrm{m,exp}} \simeq 8$ nm as a possible model, as shown in figure 11. We can introduce the formation of bundles into our MC simulation by changing the size and the aspect ratio of the constituent spherocylinders. A study of the effects of such a change in the size and aspect ratio of the spherocylinders will be a target of future simulations.

Acknowledgments

The authors gratefully acknowledge professor S Kobayashi and M Ohmae for collaborations on the experimental work cited in [4–6] which motivated the present work on MC computer simulation. This work is partially supported by Grant-in-Aid for Science from the Ministry of Education, Culture, Sports, Science and Technology, Japan.

Note added in proof. In carbohydrate chemistry, a polysaccharide refers to a compound having more than ten monosaccharide units [13]. According to this definition, the product synthesized in this study belongs to the cellulose, a typical polysaccharide family.

References

[1] Colvin J R 1959 *Nature* **183** 1135
[2] Mandelbrot B B 1982 *The Fractal Geometry of Nature* (San Francisco, CA: Freeman)
[3] Kobayashi S, Kashiwa K, Kawasaki T and Shoda S 1991 *J. Am. Chem. Soc.* **113** 3079
[4] Hashimoto T, Tanaka H, Koizumi S, Kurosaki K, Ohmae M and Kobayashi S 2006 *J. Am. Chem. Soc.* submitted
[5] Tanaka H, Hashimoto T, Koizumi S, Kurosaki K, Ohmae M and Kobayashi S 2006 *Physica* B at press
[6] Tanaka H, Hashimoto T, Koizumi S, Kurosaki K, Ohmae M and Kobayashi S 2006 *Macromolecules* submitted
[7] Ranby B G 1952 *Acta Chem. Scand.* **6** 101
[8] Porod G 1951 *Kolloidn. Zh.* **124** 83–111
[9] Bale H D and Schmidt P W 1984 *Phys. Rev. Lett.* **53** 596
[10] Schaefer D W and Keefer K D 1986 *Phys. Rev. Lett.* **56** 2199
[11] Astley O M and Donald A M 2001 *Biomacromolecules* **2** 672
[12] Lee J E, Brown R M Jr, Kuga S, Shoda S and Kobayashi S 1994 *Proc. Natl Acad. Sci. USA* **91** 7425
[13] Kennedy J F and White C A 1979 *Comprehensive Organic Chemistry* vol 5, ed D Barton, W D Ollis and E Haslam (Oxford: Pergamon) pp 755–830